Electrochimica Acta 399 (2021) 139366

Contents lists available at ScienceDirect

Electrochimica Acta

journal homepage: www.elsevier.com/locate/electacta

Dual-functional single stranded deoxyribonucleic acid for graphene oxide reduction and charge storage enhancement

Yasin Albarqouni[a], Gomaa A.M. Ali[b], Soon Poh Lee[a], Ab Rahim Mohd-Hairul[a], H. Algarni[c,d], Kwok Feng Chong[a,*]

[a] Faculty of Industrial Sciences and Technology, Universiti Malaysia Pahang, Gambang 26300, Kuantan, Malaysia
[b] Chemistry Department, Faculty of Science, Al–Azhar University, Assiut 71524, Egypt
[c] Research Centre for Advanced Materials Science (RCAMS), King Khalid University, 9004, Abha 61413, Saudi Arabia
[d] Department of Physics, Faculty of Sciences, King Khalid University, 9004, Abha 61413, Saudi Arabia

ARTICLE INFO

Article history:
Received 1 August 2021
Revised 25 September 2021
Accepted 30 September 2021
Available online 5 October 2021

Keywords:
Bioelectronics
DNA
Supercapacitor
Green reduction
Graphene

ABSTRACT

This study reports a one-step process to produce single-stranded deoxyribonucleic acid (ssDNA) functionalized reduced graphene oxide (ssDNA/rGO). The ssDNA acts as a reducing agent for the reduction of GO into rGO and simultaneously performs functionalization onto rGO, which is confirmed by spectroscopic and microscopic analyses. Such reduction capability is not being observed in double-stranded DNA (dsDNA). The high charge density of ssDNA on rGO is investigated for its application in electrochemical supercapacitor, and it is revealed that the ssDNA/rGO exhibits a specific capacitance of 129 F g^{-1} with high stability (92%) up to 10,000 cycles. The findings open the gateway to develop a biomolecule-based energy storage system.

© 2021 Elsevier Ltd. All rights reserved.

1. Introduction

Deoxyribonucleic acid (DNA) is a natural biopolymer with genetic information for the development, functioning, growth, and reproduction of all organisms. The intriguing properties of DNA have inspired its non-biological applications [1]. The molecular recognition in DNA complementary strands has been used in materials engineering at the nanometer scale, such as DNA-assisted assembly of nanoparticles into macromolecule [2], self-assembly of DNA into bulk-scale hydrogel [3], and 3D macroscopic crystals with nanoscale internal structure [4]. The electrical conductivity of DNA has also been explored for molecular electronics, where DNA has been reported to exhibit metallic-like conduction by substituting imino proton in base pairs with metal ions [5]. Due to this, DNA is incorporated into other materials for conductivity enhancement, such as DNA immobilized on polyaniline [6].

The discovery of graphene in 2004 has caused tremendous research interest due to its fascinating properties that promise massive applications in electronic, energy conversion and storage, sensing as well as catalysis [7]. The earliest approach of producing graphene by mechanical cleavage of highly ordered pyrolytic graphite is not practical for industrial mass production of graphene. Therefore, chemically modified graphene or better known as reduced graphene oxide (rGO), may provide a solution in this context. Precursor graphite is subjected to oxidation to form graphene oxide (GO), and the GO is further reduced to produce rGO [8,9]. The chemically reduced graphene oxide using hydrazine or sodium borohydride have better characteristics, however, using such hazardous reducing agents could trigger safety as well as environmental issues [10,11]. Green chemicals such as L-ascorbic acid, carotene, green tea have been proposed as the alternative reducing agent in the production of rGO [12,13].

Recent studies suggest that DNA could be an effective reducing agent, where it was used to reduce and cap the growth of gold nanowires [14]. Braun and coworkers proposed the sequence-specific molecular lithography by reducing Ag ions on the DNA backbone [15]. DNA consists of nucleobases adenine (A), guanine (G), cytosine (S), thymine (T), monosaccharide sugar, and phosphate backbone. A single-stranded DNA (ssDNA) is a polynucleotides chain with its nucleobases that are connected to one another covalently by phosphodiester linkage. A double-stranded DNA (dsDNA) is composed of two complementary polynucleotides chains that are linked by hydrogen bonds according to base pairing rules (A links with T and C links with G). Among all nucleobases, guanine has the lowest ionization potential, making it to be the easiest nucleobase to perform electron transfer in forming

* Corresponding author.
E-mail address: ckfeng@ump.edu.my (K.F. Chong).

https://doi.org/10.1016/j.electacta.2021.139366
0013-4686/© 2021 Elsevier Ltd. All rights reserved.

guanine radical cation [16]. These electron transfer properties render it to be a promising candidate as a reducing agent. This inspires us to study the reducing capability of DNA on GO in the production of rGO. The non-covalent π-π stacking between the aromatic ring of graphene and N-containing groups (purine and pyrimidine bases of DNA could promote the functionalization of DNA onto rGO [17]. Functionalized carbon materials have shown great interest as supercapacitor electrode materials [18,19]. In this work, the reducing capability of ssDNA and dsDNA on GO is investigated. It is envisaged that the DNA functionalization could occur, and the highly charged phosphate and nucleobases backbone could attract cationic electrolyte for the charge storage enhancement. To the best of our knowledge, there is no report on the comparison study in charge storage performance between ssDNA and dsDNA, which is crucial to develop a high-performance biomolecule-based energy storage device.

2. Samples preparation and characterization

2.1. Deoxyribonucleic acid (DNA) extraction

A cost-effective source of genomic DNA was obtained from cultivated *saccharomyces cerevisiae* (baking yeast) as Sambrook and Russel protocol [20]. Typically, 1 g of baking yeast was cultured in 1000 mL of Potato Dextrose Broth (PDB) media and incubated for 3 days at 35 °C. The vegetative cells were harvested by centrifuging at 6000 rpm for 5 min at 25 °C. The precipitated cells were washed by distilled water several times to eliminate any impurities that remain from the culturing media. Cell lysis was performed by adding lysis buffer before incubated in a hot water bath for 15 min at 95 °C with interval sonication and finally ended with thermal shock with an ice bath for 5 min at 0 °C. An equal volume of phenol: chloroform: isoamyl alcohol (25:24:1 v/v) was added into the lysate to partition lipids and cellular debris into the organic phase, leaving the DNA in the aqueous phase. The process of partitioning was repeated 3 times to obtain the purified DNA. Double volume of absolute ethanol was then added into the purified DNA aqueous solution and kept at −20 °C for 12 h to precipitate the DNA. The incubation for 12 h at −20 °C is to prevent the enzymatic reaction of deoxyribonuclease. The refrigerated solution was centrifuged and washed several times with 70% ethanol before vacuum drying at 60 °C to remove any impurity [21]. The dried pellet was then incubated with 500 µL TE-buffer containing (RNase A) at 35 °C for 30 min to remove any ribonucleic acid (RNA) [22]. Finally, the resulted solution was subjected to purification step using phenol:chloroform:isoamyl alcohol (25:24:1 v/v) three times to obtain the concentrated DNA. This is known as the double-stranded DNA (dsDNA), and its concentration was evaluated by applying Sambrook's protocol [23]. Single-stranded DNA (ssDNA) was obtained by denaturation of the isolated dsDNA. Typically, 50 µL of NaOH (1 mol L^{-1}) was added into 5000 µL of DNA solution with gently mixing at room temperature for 5 min before adding 50 µL of HCl (1 mol L^{-1}) [24]. A double volume of ethanol was used to concentrate the obtained ssDNA at −20 °C for 12 h, and Barbas' formula was used to evaluate the concentration [25].

2.2. GO reduction and functionalization

The graphene oxide (GO) in this study was synthesized using our previously reported method [26]. Graphite flakes (4 g) were heated at 80 °C for 6 h in the mixture of sulfuric acid (H_2SO_4) (60 mL), $K_2S_2O_8$ (6 g) and P_2O_5 (6 g). It was then diluted with 2 L of DI water, filtered, and washed until neutral pH with DI water. The collected pre-oxidized graphite was then dried in vacuum for 12 h. Then, it was further oxidized in a mixture of $KMnO_4$ (35 g) and H_2SO_4 (300 mL) at 35 °C for 4 h under stirring. The mixture was diluted with DI water (700 mL) followed by the addition of H_2O_2 (100 mL) to stop the oxidation reaction. The mixture was then filtered and washed by 1:10 HCl (5 L) and finally dried in vacuum for 12 h to obtain graphite oxide. The graphite oxide was exfoliated by sonicating graphite oxide dispersion (2 mg mL^{-1}) for 30 min. The unexfoliated graphite oxide was removed by centrifugation as precipitate and the homogenous yellow supernatant was obtained as graphene oxide (GO) dispersion. For the reduction of GO by DNA, mass ratio of 1:4 (dsDNA or ssDNA: GO) was used. The ssDNA and dsDNA solution were separately added into GO dispersions and heated at 80 °C under stirring condition. This temperature was chosen to avoid the denaturation of DNA. The reaction mixture was then filtered, washed, and dried in vacuum for 12 h. They are denoted as ssDNA/rGO and dsDNA/GO.

2.3. Structural and morphological characterizations

The UV absorbance of DNA in this work was investigated by using microvolume spectrophotometer (NanoDrop™ 2000/2000c, Thermo Fisher Scientific CO.). The denaturation percentage of ds-DNA into ssDNA was determined by Eq. (1) [27].

$$\text{Denaturation}\,(\%) = \left[\frac{A_{260}(\text{Final}) - A_{260}(\text{Blank})}{A_{260}(\text{Initial})} - 1\right] \times 200 \quad (1)$$

Where A_{260}(Initial) is the absorbance of dsDNA before denaturation; A_{260}(Final) is the absorbance of ssDNA after denaturation and A_{260}(Blank) is the absorbance of blank. The functional groups were studied by a Fourier transformed infrared spectrometer in Attenuated Total Reflectance mode (ATR-FTIR, Spectrum 100, PerkinElmer). The electronic transition of samples was studied by UV–Vis spectrophotometer (CARY, AGILENT). X-ray diffraction pattern (XRD) was collected by a Rigaku X-ray diffractometer (Miniflex II with Cu-Kα radiation at 30 kV, 15 mA, λ = 1.5406 Å) within the 2θ range of 3° to 80° The Raman spectra were collected by Raman spectrometer (Renishaw, inVia Reflex) with 2.33 eV (532 nm) laser energy. The sample morphology was investigated by a field emission scanning electron microscope (FESEM, JSM-7800F, JEOL). The DNA staining was performed with Diamond™ Nucleic Acid Dye and visualized by a chromophore imaging system (GE AI600 RGB GEL Imaging System).

2.4. Electrochemical characterization

The electrochemical experiment was conducted by an electrochemical workstation (AUTOLAB PGSTAT30, Metrohm) equipped with a frequency response analyzer. The charge storage properties were investigated by cyclic voltammetry (CV), galvanostatic charge-discharge (GCD), and electrochemical impedance spectroscopy (EIS) in three-electrode system. The working electrodes were prepared by mixing the samples (90 wt%), carbon black (5.0 wt%; Alfa Aesar) and polyvinylidene difluoride (PVDF, 5.0 wt%) in N-methyl-2-pyrrolidinone (NMP), followed by pressing onto a piece of pre-treated Ni foam [28] and then dried at 70 °C in a vacuum oven for 24 h. Pt wire and Ag/AgCl were used as counter and reference electrode, respectively.

3. Results and discussion

3.1. Structural and morphological characterizations

The dsDNA in this work was extracted from baker's yeast and denatured to produce ssDNA. The denaturation degree was quantified by investigating the hyperchromic effect in UV analysis [27] (supplementary Fig. S1), and it was found out that a high percentage of dsDNA (98.24%) had been denatured into ssDNA

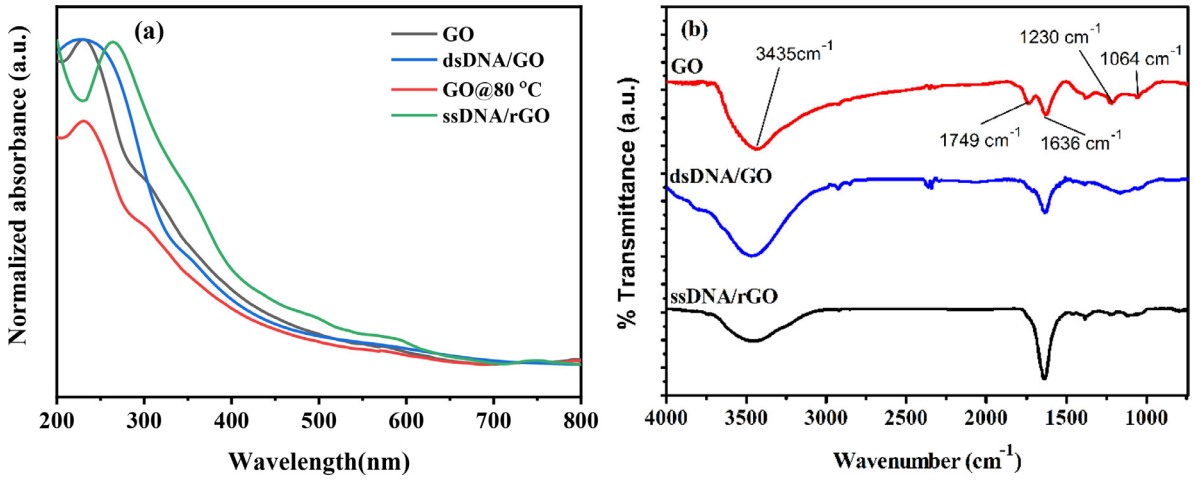

Fig. 1. (a) UV–Vis spectra of GO, dsDNA/GO, ssDNA/rGO and GO@ 80 °C (control); (b) FTIR spectra of GO, dsDNA/GO and ssDNA/rGO.

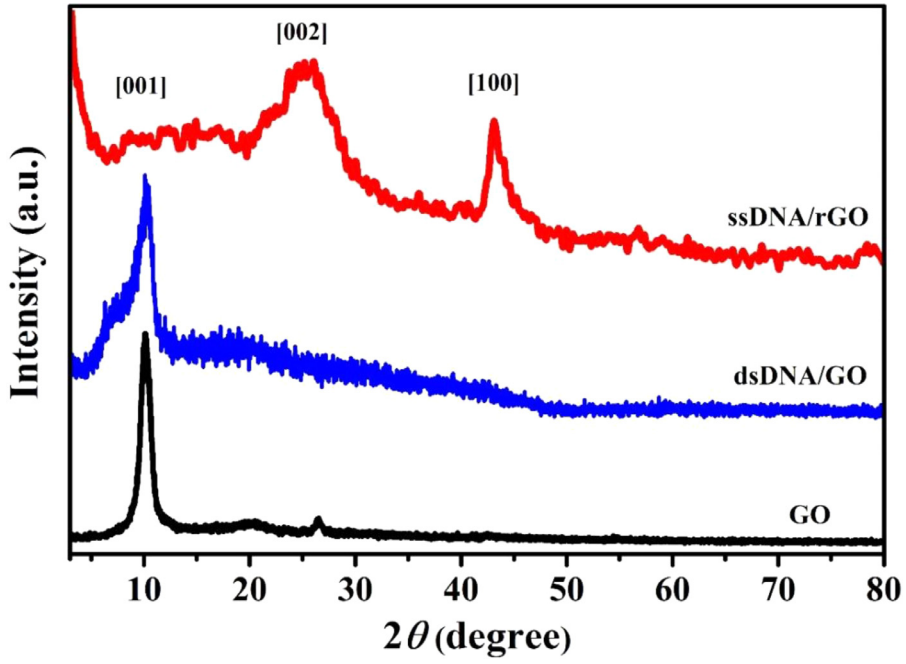

Fig. 2. XRD patterns for GO, dsDNA/GO, and ssDNA/rGO.

(Detailed calculation in Supporting Information). ATR-FTIR analysis (supplementary supplementary Fig. S2) also provides evidence for the denaturation of dsDNA into ssDNA. The absorption bands at 1698 and 1553 cm^{-1} are corresponding to the *C=O* and $-NH_2$ in dsDNA, respectively [29–31]. After denaturation into ssDNA, the two peaks shift to higher wavenumber (1700 cm^{-1} for *C=O* and 1565 cm^{-1} for $-NH_2$). These up-shifted peaks indicate the fast vibration of carbonyl stretching and amide bending, which may be attributed to the absence of hydrogen bonds between carbonyl and amide groups in ssDNA [27]. Upon unwinded (denatured) of dsDNA into ssDNA, the FTIR peak for *C=O* and -NH_2 shifted to the longer wavenumber which had been reported elsewhere [31,32].

The dsDNA and ssDNA were added into GO solution and incubated at 80 °C for the reduction process. In UV spectrum (Fig. 1a), GO exhibits an absorption peak at 230 nm that indicates the $\pi-\pi^*$ transition of the aromatic rings. Besides, a broad shoulder peak in the range of

(290–309 nm) is attributed to the presence of peroxide- and epoxides-like linkages [33]. After incubating with ssDNA, this oxygen-related broad shoulder peak disappears and the $\pi-\pi^*$ peak shifts from 230 nm to 270 nm, indicating the restoration of π conjugation network by ssDNA to form ssDNA/rGO [34]. On the other hand, the incubation of dsDNA with GO does not produce significant changes where the $\pi-\pi^*$ peak only shifts to 258 nm. It shows the low ability of dsDNA to reduce GO. Control experiment (GO@80 °C) was conducted to eliminate the heat (80 °C) factor in contributing to the reduction process. It is clear that the $\pi-\pi^*$ peak remains at 230 nm, in the case of incubating GO only at 80 °C. It shows that ssDNA is the main contributing factor in reducing GO into rGO. The reduction effect of ssDNA can also be observed at FTIR analysis (Fig. 1b). As compared to GO, all the oxygen related peaks (O–H at ca. 3435 cm^{-1}; *C=O* at ca. 1749 cm^{-1}; C–O at 1230 cm^{-1} and 1064 cm^{-1}) have been reduced for ssDNA/rGO. The extent of reduction in ssDNA/rGO is greater than dsDNA/GO. It can be seen that the restoration of *C=C* upon oxygen groups removal is more prominent at ssDNA/rGO as the *C=C* peak (at ca. 1636 cm^{-1}) is having highest intensity.

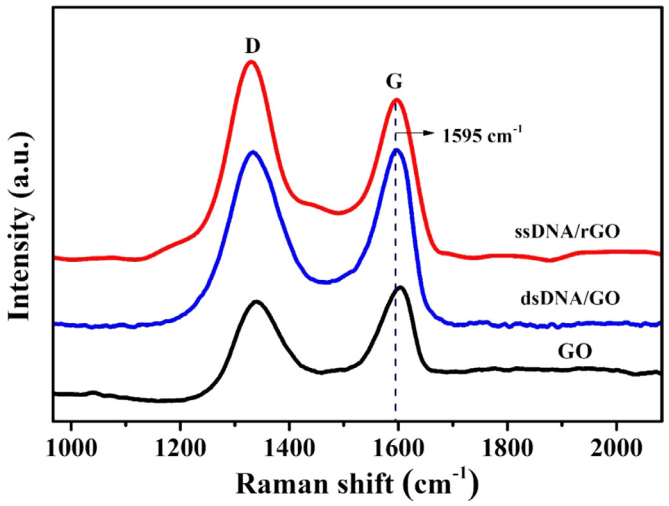

Fig. 3. Raman spectra for GO, dsDNA/GO, and ssDNA/rGO.

In XRD analysis (Fig. 2), GO exhibits a sharp peak (001) at $2\theta = 10.1°$, corresponds to the interlayer spacing (d spacing) of ca. 0.87 nm. Upon incubation with ssDNA, the ssDNA/rGO shows diffraction peaks of (002) and (100), at $2\theta = 25.3°$ and 42.5°, respectively. It also corresponds to a D-spacing of 0.36 nm. The reduced D-spacing in ssDNA/rGO may be attributed to the removal of oxygen groups in GO [35]. On the other hand, the incubation of dsDNA with GO does not produce significant changes to its crystal structure, with a diffraction peak (001) at $2\theta = 10.3°$. The XRD findings corroborate to the UV analysis that proves the reduction of GO by ssDNA. The reaction time between GO and ssDNA was investigated, and it was concluded that 90 min reaction could produce optimized reduction as proven by the disappearing of 001 and appearing of 002 diffraction peak (supplementary Fig. S3)

It is generally known that GO possesses high number of defect sites due to multiple oxidation process [36]. The number of defect sites is reduced after sp^2 carbon network restoration in rGO and I_D/I_G ratio in Raman spectrum (Fig. 3) can provide important information on this. Higher I_D/I_G indicates higher number of defect sites [37]. The Raman spectrum of ssDNA/rGO shows the increment of I_D/I_G ratio (1.13), as compared to that of GO (0.90). This indicates higher defect sites are created during reduction of GO into rGO. This reduction process is categorized as the chemical reduction method which produces defect sites in rGO as compared to other methods for graphene production (mechanical exfoliation and CVD [38]). Furthermore, the presence of DNA also contributes the increase of Raman signal in the region of 1314 cm^{-1}. It is worth noting that there is a redshift of the G band for both ssDNA/rGO and dsDNA/GO, as compared to that of GO. The redshift can be associated to the charge transfer between ssDNA and rGO as well as dsDNA and GO [39]. Similar findings had been reported on DNA-GO hydrogel and CNT wrapped with DNA [40,41]. This observation suggests the possibility of DNA functionalization on the graphene basal plane *via* π-π stacking interactions between nucleobases of DNA and graphene structure [42], which is worth further investigation.

The existence of ssDNA on rGO was investigated by fixation with Diamond™ Nucleic Acid Dye, where the dye binding to DNA can be visualized under UV illumination (Fig. 4). It can be clearly seen that both ssDNA/rGO and dsDNA/GO exhibit dye staining, an evidence of ssDNA and dsDNA functionalization onto rGO and GO, respectively. It could be attributed to the presence of aromatic rings in DNA that interacts with the aromatic structure of GO or rGO throwgh π–π stacking [43]. Control experiment on GO sample shows that the staining on ssDNA/rGO and dsDNA/GO are originated from the dye binding with ssDNA and dsDNA. All the spectroscopy analyses conclude that ssDNA could reduce GO into rGO and simultaneously functionalize on rGO to form ssDNA/rGO. The *saccharomyces cerevisiae*'s genome has been reported to possess a high percentage of guanine (36%), which exhibits the lowest oxidation potential among four DNA bases [44]. This makes guanine could act as the reducing agent to reduce GO into rGO. However, the double helix structure of dsDNA creates steric hindrance that blocks the guanine from accessing to GO surface for the reduction process. It explains the inability of dsDNA in reducing GO into rGO, as shown from the spectroscopy analyses. On the contrary, the single strand structure in ssDNA allows guanine to facilely access to the GO surface to perform reduction. In addition, it has been reported that ssDNA possesses enzymatic-like capability as DNAzyme to catalyze a designed process. Both ssDNA/rGO and dsDNA/GO exist as thin and wrinkle sheet morphology (Fig. 5) that are produced during oxidation process. The presence of DNA is not visible under FESEM observation.

3.2. Electrochemical characterization

The charge storage capability of ssDNA/rGO was investigated using CV, CDC, and EIS in 3-electrode setup. The ssDNA/rGO was proposed as the negative electrode and its charge storage was studied in the cathodic region. Previous report suggested that the cathodic region is more preferred for ssDNA because of its negatively charged phosphate and nitrogen-containing nucleobases prefer cationic electrolytes over anionic ones [45]. Fig. 6a,b show the CV curves of ssDNA/rGO in 1 M KOH and 1 M Na_2SO_4 at different scan rates. In addition, CV at 50 mV s^{-1} is shown for ssDNA/rGO in both KOH and Na_2SO_4 electrolytes (Fig. 6c) for

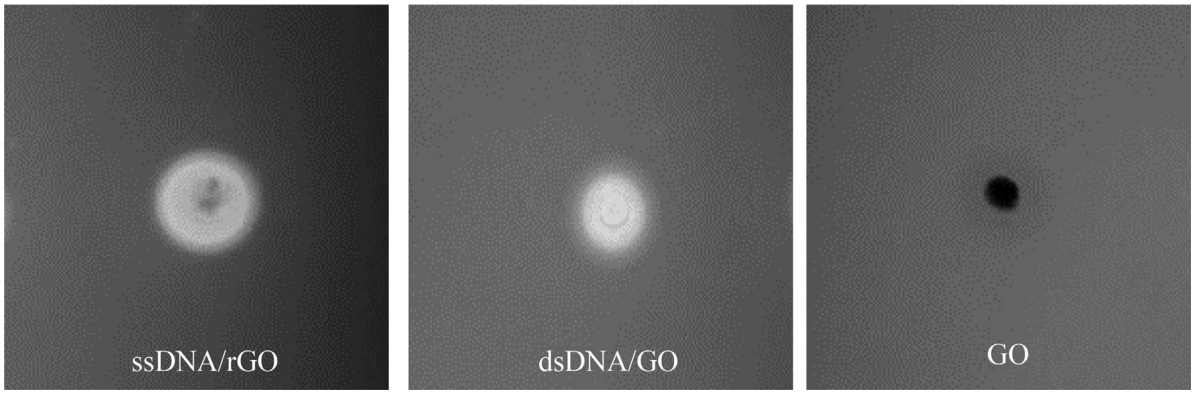

Fig. 4. DNA staining visualization ssDNA/rGO, dsDNA/GO and GO (control).

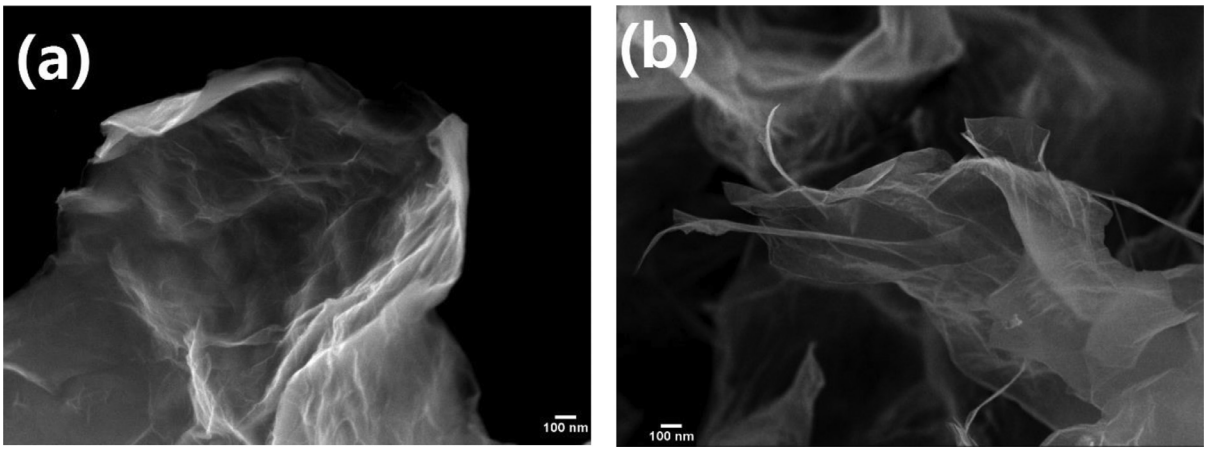

Fig. 5. Surface morphological investigation using FESEM for (a) ssDNA/rGO and (b) dsDNA/GO.

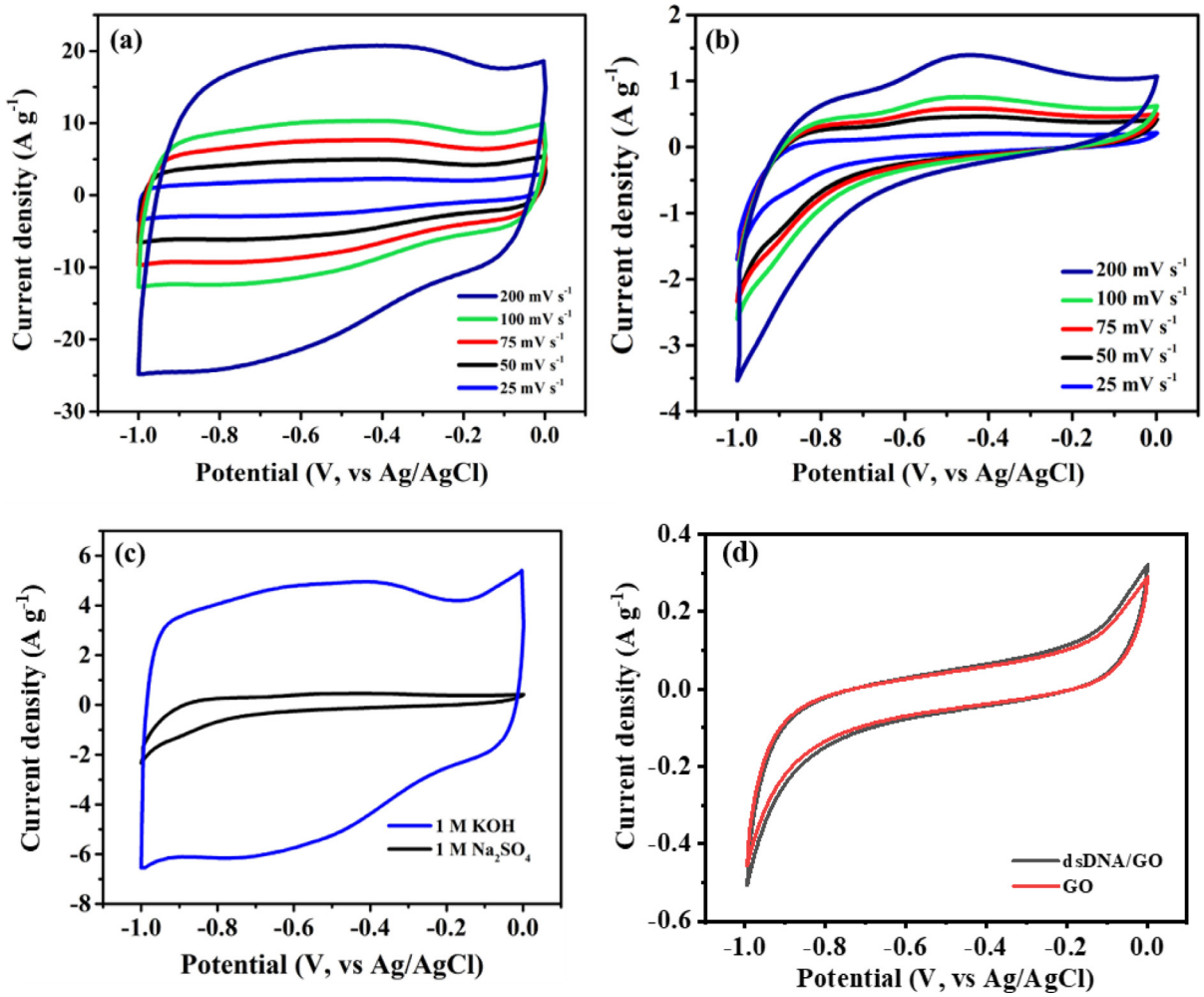

Fig. 6. CV curves at different scan rates for ssDNA/rGO in (a) 1 M KOH and (b) 1 M Na_2SO_4, (c) CV curves for ssDNA/rGO in Na_2SO_4 and KOH at 50 mV s^{-1}, (d) CV comparison between GO, dsDNA/GO at 50 mV s^{-1}.

comparison. Na_2SO_4 is widely used as the neutral electrolyte for biomolecule-based material while KOH is used as basic electrolyte that has higher capacitive performance at comparatively lower potential window stability [46,47]. ssDNA/rGO manifests redox peaks (−0.5 to −0.6 V) in both KOH and Na_2SO_4 electrolyte which could be attributed to the redox reaction of phosphate group and nucleobases. The area under the curve provides an indication of the charge storage where a larger area represents higher charge storage [48]. It is evident that ssDNA/rGO shows larger CV area in the KOH electrolyte, which signifies higher charge storage in it. This phenomenon could be explained by the higher molar conductivity of K^+ ions (7.35 mS m^2 mol^{-1}) as compared to that of Na^+ ions (5.01 mS m^2 mol^{-1}) [49,50]. Hence, the following electrochemical experiment was conducted in KOH electrolyte. CV curves

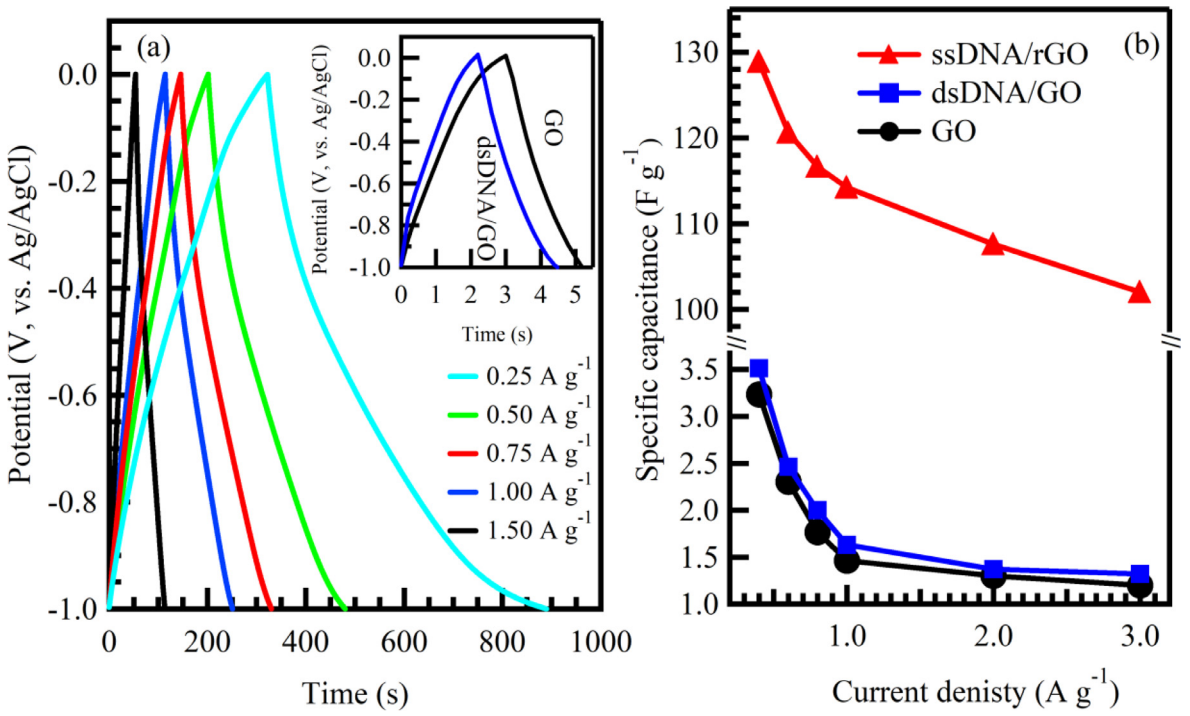

Fig. 7. (a) GCD curves of ssDNA/rGO in 1 M KOH at different current densities; Inset compares GCD for GO and dsDNA/GO at 1 A g^{-1} (b) Calculated specific capacitance for ssDNA/rGO, dsDNA/GO and GO at different current densities.

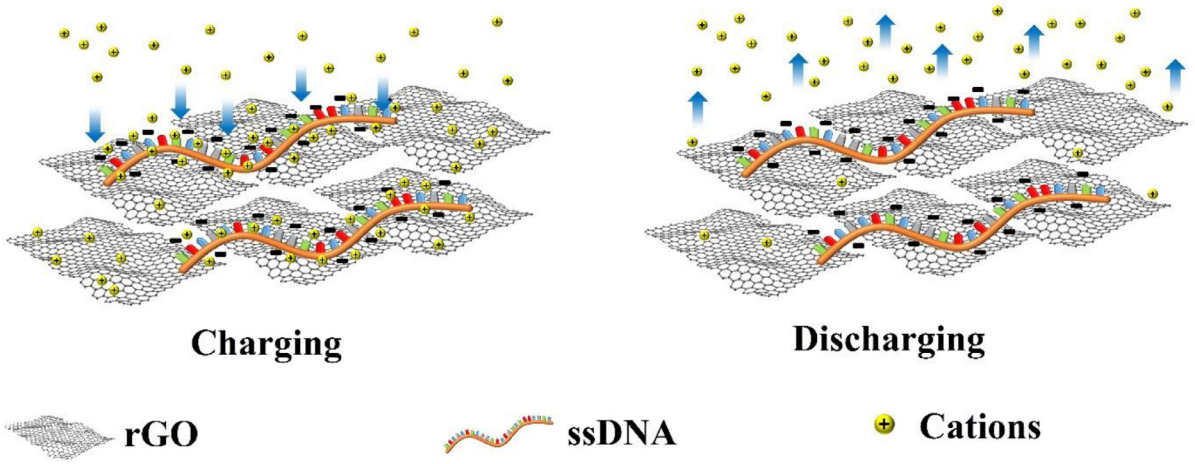

Schematic 1. Illustration of the cations migration on negatively charged ssDNA/rGO electrode during charging and discharging process.

of dsDNA/GO and GO are presented at Fig. 6d, where the CV of dsDNA/GO does not show significant change as compared to that of GO. It is worth mentioning that ssDNA/rGO exhibits an exceptionally larger CV area as compared to that of dsDNA/GO, indicating higher charge storage in ssDNA/rGO. As mentioned earlier, the presence of phosphate and nucleobase redox reactions could contribute to pseudocapacitance for charge storage. However, this redox reaction can only be seen on ssDNA, but not dsDNA. This phenomenon could be explained by referring to the structure of dsDNA, which consists of two DNA strands connect with each other by hydrogen bonding. This double-stranded nature blocks the access of cation to the phosphate and nucleobases as the hydrated cation K^+ (3.31 nm) and Na^+ (3.58 nm) are bigger than the spacing between DNA strands in dsDNA (1.86 Å) [51,52]. CV curves of GO and bare nickel foam are shown as supplementary Fig. S4, to show the low contribution of charge storage from nickel foam.

The GCD technique simulates a real application of supercapacitor to attract the ions during charging and release the ions during discharging. The GCD curves of ssDNA/rGO in KOH electrolyte at different current densities are shown in Fig. 7a. The charging and discharging curves are symmetrical at different current densities, indicating the reversibility of ssDNA/rGO in charge storage process. For comparison, the GCD curves at 1 A g^{-1} of dsDNA/GO and GO are presented as Fig. 7a inset that show the short discharge time or lower capacitance. The specific capacitance values are computed by dividing the current density with discharge curve slope [28,53] and they are summarized in Fig. 7b. The highest specific capacitance of 129 F g^{-1} is attained on ssDNA/rGO at 0.4 A g^{-1}, which is about 32 times higher than that of dsDNA/GO (3.5 F g^{-1}). The enhancement of specific capacitance can be visualized as Schematic 1. During charging process from 0 to −1.0 V, K^+ ions migrate to the electrode surface. On ssDNA/rGO, the negative charge on phosphate and nucleobases are exposed which attract more

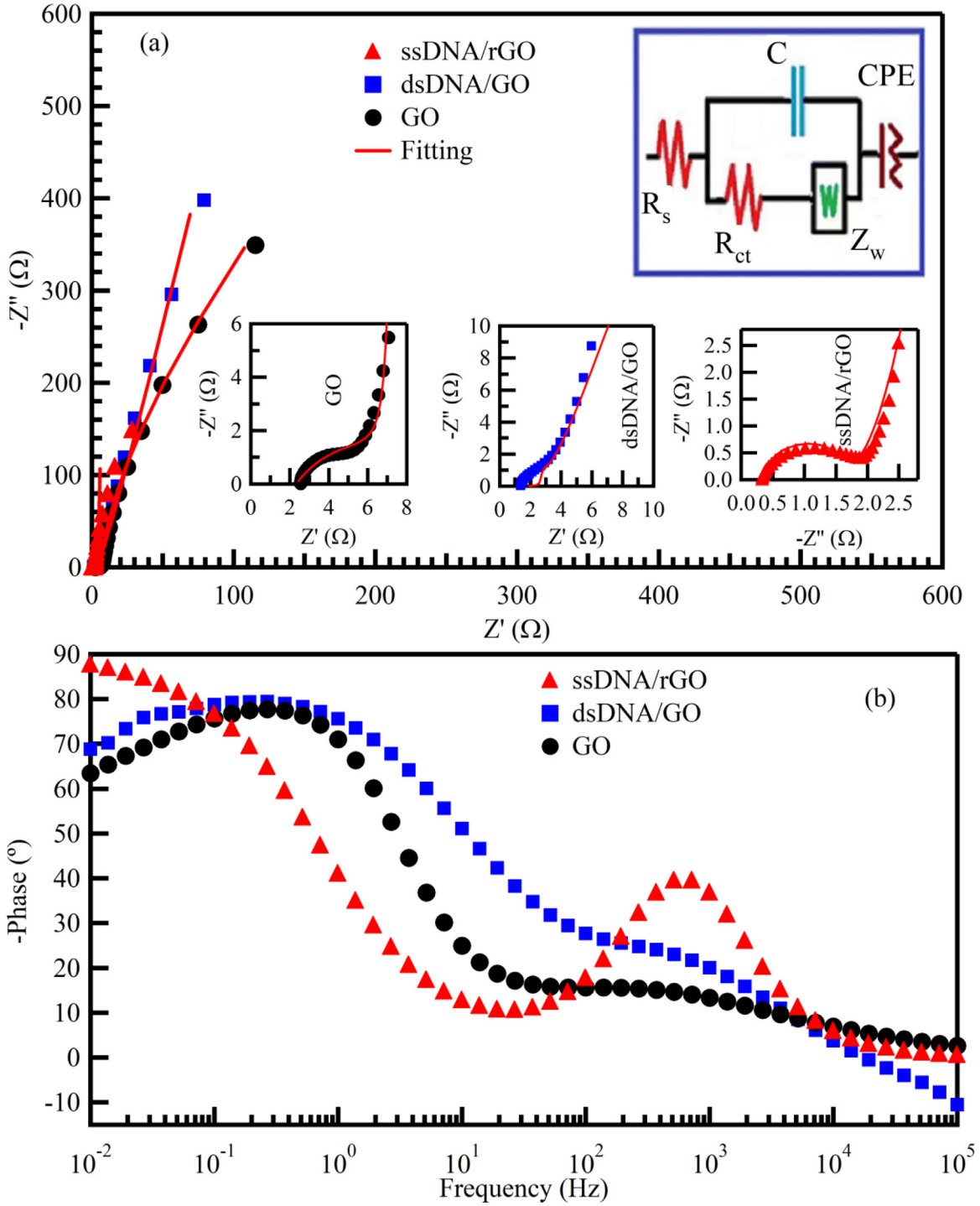

Fig. 8. (a) Nyquist plots for ssDNA/rGO, dsDNA/GO and GO; insets show the low frequency regions and fitting circuit. (b) Bode plots for ssDNA/rGO, dsDNA/GO and GO.

positive K^+ ions on ssDNA/rGO surface. It creates higher ions adsorption for EDLC effect. Furthermore, the ions interaction with exposed phosphate and nucleobases in ssDNA renders redox reaction that contributes to pseudocapacitance effect. The higher conductivity of rGO also promotes charge propagation within the electrode. All these promote the charge storage activity in ssDNA/rGO. On the other hand, the dsDNA in dsDNA/rGO exists as a double helix form where phosphate and nucleobases are shielded from the K^+ ions. It creates less attraction towards K^+ ions for ions adsorption and redox activity. Most importantly, the unreduced GO possesses weak conductivity that limits the charge propagation and lower charge storage is manifested. For both materials, the K^+ ions are released from electrode during discharge process from −1.0 to 0 V. Table 1 shows the electrochemical performance comparison with other DNA-based supercapacitor electrode.

Electrochemical impedance spectroscopy (EIS) was used to investigate the charging kinetics of the electrode. Fig. 8a shows the Nyquist plots of ssDNA/rGO, dsDNA/GO, and GO, with the equivalent circuit fitting as inset. The EIS fitted data is tabulated as Table 2. It is worth noting that the *Rs* value for ssDNA/rGO (0.40 Ω) is much lower as compared to that for dsDNA/GO (1.39 Ω). It corroborates to the findings that ssDNA reduces GO into highly con-

Table 1
Comparison of reported specific capacitance obtained for ssDNA/rGO with other related graphene-based nanocomposites.

Composite	DNA source	C_s (F g^{-1})	Reference
SWCNT@DNA fiber	salmon sperm DNA, 10,000 (bp)	60.0	[54]
CNTs @DNA	ssDNA ~ 200 bp	124.6	[49]
SnO_2 @DNA	dsDNA herring testes ~ 50 K bp	126.0	[55]
Graphene modified Guanine	Guanine	197.8	[56]
$NiCo_2O_4$–MWCNTs@DNA	salmon DNA, 200 (bp)	223.7	[57]
rGO/ssDNA	Yeast ssDNA	129.0	This work

Table 2
The calculated parameters obtained by fitting the experimental impedance data of ssDNA/rGO and dsDNA/GO electrodes.

	R_S (Ω)	R_{CT} (Ω)	C (mF)	CPE (Ω^{-1} s^n)	W (Ω)	S_E (m^2 g^{-1})	χ^2
ssDNA/rGO	0.40	1.35	0.413	0.110	0.036	490.6	0.234
dsDNA/GO	1.39	1.51	0.200	0.040	0.06	163.9	0.322
GO	2.44	3.28	0.005	0.092	0.198	142.1	0.162

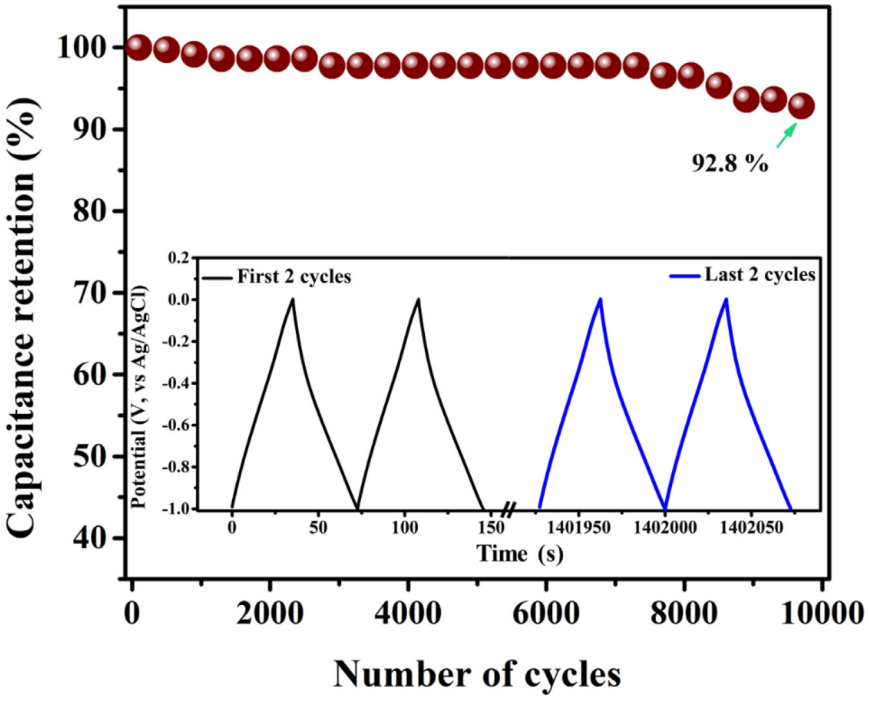

Fig. 9. Cycling stability of ssDNA/rGO electrode in 1 M KOH electrolyte at 3 A g^{-1}. The inset shows the GCD curves for the first and last 2 cycles.

ductive rGO while dsDNA does not perform such reduction on GO. The higher ions adsorption on ssDNA/rGO can be seen from higher *CPE* and *C* values, which supports the findings for ions-attracting ssDNA. The electroactive surface area (S_E) is calculated from equation $S_E=C_{dm}/C_d$ [58,59], where $C_{dm}=(2\pi f mZ")^{-1}$, Z" is the imaginary impedance from Nyquist plots at frequency 0.01 Hz and C_d is a constant value of 20 μF cm^{-2} for carbonaceous materials [60]. Interestingly, ssDNA/rGO demonstrates a high S_E of 490.6 m^2 g^{-1}, which is about 3 times higher than that of dsDNA/GO (163.9 m^2 g^{-1}). It can be associated to the exposed phosphate and nucleobases in ssDNA that provide higher electroactive sites. The charge storage behavior of ssDNA/rGO can also be observed from the Bode plot (Fig. 8b) where it shows phase angle of 88.4° at low frequency, very close to the phase angle of the ideal capacitance of 90° dsDNA/GO only shows phase angle of 68.6° at low frequency. The high-performance ssDNA/rGO was further tested for their long term stability at continuous GCD for 10,000 cycles. Fig. 9 shows that ssDNA/rGO could retain up to 92.80% specific capacitance after 10,000 GCD cycles. The inset shows the GCD curves do not change significantly after the stability test, suggesting the high stability of ssDNA/rGO as supercapacitor electrode.

4. Conclusions

The present work demonstrates the ssDNA could be used as an effective reducing agent for GO reduction. The low oxidation potential of guanine in DNA possesses reducing capability and the single-stranded form in ssDNA renders the guanine to be exposed to reduce the GO sheets. This phenomenon can only be observed on ssDNA, where the reducing capability is reduced on dsDNA that may be attributed to the shielded guanine in double-stranded form of dsDNA. However, the DNA functionalization on GO or rGO occurs due the π–π interaction between graphene's aromatic rings and DNA's nucleobases. The negatively charged ssDNA functionalization onto rGO contributes to the charge storage enhancement, in addition to the double layer capacitance contributed by the rGO. The dual functionality of ssDNA in GO reduction and charge storage enhancement can stimulate a new research doorway to facil-

itate the biomolecule-based supercapacitor by harnessing the outstanding properties of DNA.

Declaration of Competing Interest

The authors declare no competing financial interests.

Credit authorship contribution statement

Yasin Albarqouni: Methodology, Data curation, Writing – original draft. **Gomaa A.M. Ali:** Conceptualization, Formal analysis, Data curation, Writing – original draft. **Soon Poh Lee:** Methodology, Data curation, Writing – original draft. **Ab Rahim Mohd-Hairul:** Methodology, Data curation, Writing – original draft. **H. Algarni:** Methodology, Data curation, Writing – original draft. **Kwok Feng Chong:** Conceptualization, Methodology, Data curation, Writing – original draft.

Acknowledgments

The authors would like to acknowledge the funding from the Ministry of Higher Education, Malaysia in the form of [RDU1901186:FRGS/1/2019/STG07/UMP/02/6] and Malaysia Toray Science Foundation grant RDU201502. In addition, H. Algarni extends his appreciation to the Deanship of Scientific Research at King Khalid University for funding this work through the research group project under grant number (KKU/RCAMS/G0014/21).

Supplementary materials

Supplementary material associated with this article can be found, in the online version, at doi:10.1016/j.electacta.2021.139366.

References

[1] D. Yang, M.R. Hartman, T.L. Derrien, S. Hamada, D. An, K.G. Yancey, R. Cheng, M. Ma, D. Luo, DNA materials: bridging nanotechnology and biotechnology, Acc. Chem. Res. 47 (2014) 1902–1911.
[2] C. Zhu, M. Wang, J. Dong, C. Zhou, Q. Wang, Modular assembly of plasmonic nanoparticles assisted by DNA origami, Langmuir 34 (2018) 14963–14968.
[3] Y. Shao, H. Jia, T. Cao, D. Liu, Supramolecular hydrogels based on DNA self-assembly, Acc. Chem. Res. 50 (2017) 659–668.
[4] Z. Li, L. Liu, M. Zheng, J. Zhao, N.C. Seeman, C. Mao, Making engineered 3D DNA crystals robust, J. Am. Chem. Soc. 141 (2019) 15850–15855.
[5] S.Ram Kumar Pandian, C.J. Yuan, C.C. Lin, W.H. Wang, C.C. Chang, DNA-based nanowires and nanodevices, Adv. Phys.: X 2 (2017) 22–34.
[6] J. Hur, K. Im, S.W. Kim, U.J. Kim, J. Lee, S. Hwang, J. Song, S. Kim, S. Hwang, N. Park, DNA hydrogel templated carbon nanotube and polyaniline assembly and its applications for electrochemical energy storage devices, J. Mater. Chem. A 1 (2013) 14460–14466.
[7] S.K. Tiwari, S. Sahoo, N. Wang, A. Huczko, Graphene research and their outputs: status and prospect, J. Sci.: Adv. Mater. Devices 5 (2020) 10–29.
[8] A.M. Dimiev, J.M. Tour, Mechanism of graphene oxide formation, ACS Nano 8 (2014) 3060–3068.
[9] G.A.M. Ali, S.A. Makhlouf, M.M. Yusoff, K.F. Chong, Structural and electrochemical characteristics of graphene nanosheets as supercapacitor electrodes, Rev. Adv. Mater. Sci. 40 (2015) 35–43.
[10] S. Park, J. An, J.R. Potts, A. Velamakanni, S. Murali, R.S. Ruoff, Hydrazine-reduction of graphite- and graphene oxide, Carbon 49 (2011) 3019–3023.
[11] M.J. Fernández-Merino, L. Guardia, J.I. Paredes, S. Villar-Rodil, P. Solís-Fernández, A. Martínez-Alonso, J.M.D. Tascón, Vitamin C is an ideal substitute for hydrazine in the reduction of graphene oxide suspensions, J. Phys. Chem. C 114 (2010) 6426–6432.
[12] M.T.H. Aunkor, I.M. Mahbubul, R. Saidur, H.S.C. Metselaar, The green reduction of graphene oxide, RSC Adv. 6 (2016) 27807–27825.
[13] Y.M.Y. Albarqouni, S.P. Lee, G.A.M. Ali, A.S. Ethiraj, H. Algarni, K.F. Chong, Facile synthesis of reduced graphene oxide aerogel in soft drink as supercapacitor electrode, J. Nanostruct. Chem. (2021), doi:10.1007/s40097-021-00424-7.
[14] T. Bayrak, S. Helmi, J. Ye, D. Kauert, J. Kelling, T. Schönherr, R. Weichelt, A. Erbe, R. Seidel, DNA-Mold templated assembly of conductive gold nanowires, Nano Lett. 18 (2018) 2116–2123.
[15] A. Tanaka, Y. Matsuo, Y. Hashimoto, K. Ijiro, Sequence-specifically platinum metal deposition on enzymatically synthesized DNA block copolymer, Chem. Commun. 297 (2008) 4270–4272.
[16] R. Chakraborty, S. Bose, D. Ghosh, Effect of solvation on the ionization of guanine nucleotide: a hybrid QM/EFP study, J. Comput. Chem. 38 (2017) 2528–2537.
[17] V. Georgakilas, J.N. Tiwari, K.C. Kemp, J.A. Perman, A.B. Bourlinos, K.S. Kim, R. Zboril, Noncovalent functionalization of graphene and graphene oxide for energy materials, biosensing, catalytic, and biomedical applications, Chem. Rev. 116 (2016) 5464–5519.
[18] L. Ma, Z. Bi, W. Zhang, Z. Zhang, Y. Xiao, H. Niu, Y. Huang, Synthesis of a three-dimensional interconnected oxygen-, boron-, nitrogen-, and phosphorus tetratomic-doped porous carbon network as electrode material for the construction of a superior flexible supercapacitor, ACS Appl. Mater. Interfaces 12 (2020) 46170–46180.
[19] L. Ma, Z. Bi, Y. Xue, W. Zhang, Q. Huang, L. Zhang, Y. Huang, Bacterial cellulose: an encouraging eco-friendly nano-candidate for energy storage and energy conversion, J. Mater. Chem. A 8 (2020) 5812–5842.
[20] J. Sambrook, D.W. Russell, Rapid amplification of 5′ cDNA ends (5′-RACE), Cold Spring Harb. Protoc. 2006 (2006), doi:10.1101/pdb.prot3989.
[21] M.R. Green, J. Sambrook, Rapid Isolation of yeast DNA, Cold Spring Harb. Protoc. 2018 (2018).
[22] C. Tong, C. Zhao, B. Liu, B. Li, Z. Ai, J. Fan, W. Wang, Sensitive detection of RNase A activity and collaborative drug screening based on rGO and fluorescence probe, Anal. Chem. 90 (2018) 2655–2661.
[23] J. Sambrook, D.W. Russel, Molecular cloning, 3-volume set: a laboratory manual, 2000.
[24] X. Wang, H.J. Lim, A. Son, Characterization of denaturation and renaturation of DNA for DNA hybridization, Environ. Health Toxicol. 29 (2014) e2014007-e2014007.
[25] C.F. Barbas, D.R. Burton, J.K. Scott, G.J. Silverman, Quantitation of DNA and RNA, Cold Spring Harb. Protoc. 2007 (2007), doi:10.1101/pdb.ip1147.
[26] S.P. Lee, G.A.M. Ali, H. Algarni, K.F. Chong, Flake size-dependent adsorption of graphene oxide aerogel, J. Mol. Liq. 277 (2019) 175–180.
[27] X. Wang, A. Son, Effects of pretreatment on the denaturation and fragmentation of genomic DNA for DNA hybridization, Environ. Sci.: Processes Impacts 15 (2013) 2204–2212.
[28] G.A.M. Ali, M.R. Thalji, W.C. Soh, H. Algarni, K.F. Chong, One-step electrochemical synthesis of MoS_2/graphene composite for supercapacitor application, J. Solid State Electrochem. 24 (2020) 25–34.
[29] M.L.S. Mello, B.C. Vidal, Changes in the infrared microspectroscopic characteristics of DNA caused by cationic elements, different base richness and single-stranded form, PLoS One 7 (2012) e43169-e43169.
[30] D.R. Whelan, K.R. Bambery, P. Heraud, M.J. Tobin, M. Diem, D. McNaughton, B.R. Wood, Monitoring the reversible B to A-like transition of DNA in eukaryotic cells using Fourier transform infrared spectroscopy, Nucleic Acids Res. 39 (2011) 5439–5448.
[31] H. Fritzsche, A. Akhebat, E. Taillandier, K. Rippe, T.M. Jovin, Structure and drug interactions of parallel-stranded DNA studied by infrared spectroscopy and fluorescence, Nucleic Acids Res. 21 (1993) 5085–5091.
[32] G. Giubertoni, O.O. Sofronov, H.J. Bakker, Effect of intramolecular hydrogen-bond formation on the molecular conformation of amino acids, Commun. Chem. 3 (2020) 84.
[33] E. Rommozzi, M. Zannotti, R. Giovannetti, C.A. D'amato, S. Ferraro, M. Minicucci, R. Gunnella, A. Di Cicco, Reduced graphene oxide/TiO_2 nanocomposite: from synthesis to characterization for efficient visible light photocatalytic applications, Catalysts 8 (2018) 598.
[34] G.B. Mahendran, S.J. Ramalingam, J.B.B. Rayappan, S. Kesavan, T. Periathambi, N. Nesakumar, Green preparation of reduced graphene oxide by Bougainvillea glabra flower extract and sensing application, J. Mater. Sci.: Mater. Electron. 31 (2020) 14345–14356.
[35] L. Gan, B. Li, Y. Chen, B. Yu, Z. Chen, Green synthesis of reduced graphene oxide using bagasse and its application in dye removal: a waste-to-resource supply chain, Chemosphere 219 (2019) 148–154.
[36] N. Sharma, V. Sharma, R. Vyas, M. Kumari, A. Kaushal, R. Gupta, S.K. Sharma, K. Sachdev, A new sustainable green protocol for production of reduced graphene oxide and its gas sensing properties, J. Sci.: Adv. Mater. Devices 4 (2019) 473–482.
[37] E. Dervishi, Z. Ji, H. Htoon, M. Sykora, S.K. Doorn, Raman spectroscopy of bottom-up synthesized graphene quantum dots: size and structure dependence, Nanoscale 11 (2019) 16571–16581.
[38] B.-J. Park, J.-S. Choi, J.-H. Eom, H. Ha, H.Y. Kim, S. Lee, H. Shin, S.-G. Yoon, Defect-free graphene synthesized directly at 150 °C via Chemical vapor deposition with no transfer, ACS Nano. 12 (2018) 2008–2016.
[39] B. Das, R. Voggu, C.S. Rout, C.N.R. Rao, Changes in the electronic structure and properties of graphene induced by molecular charge-transfer, Chem. Commun. (2008) 5155–5157.
[40] Y. Xu, Q. Wu, Y. Sun, H. Bai, G. Shi, Three-dimensional self-assembly of graphene oxide and DNA into multifunctional hydrogels, ACS Nano 4 (2010) 7358–7362.
[41] A. Erdem, P. Papakonstantinou, H. Murphy, Direct DNA hybridization at disposable graphite electrodes modified with carbon nanotubes, Anal. Chem. 78 (2006) 6656–6659.
[42] Y. Hu, F. Li, X. Bai, D. Li, S. Hua, K. Wang, L. Niu, Label-free electrochemical impedance sensing of DNA hybridization based on functionalized graphene sheets, Chem. Commun. 47 (2011) 1743–1745.
[43] S. Kundu, A. Pyne, R. Dutta, N. Sarkar, Unveiling the interaction of duplex DNA with graphene oxide in the presence of two diverse binders: a detailed photophysical study, J. Phys. Chem. C 122 (2018) 6876–6888.
[44] C.E. Crespo-Hernández, D.M. Close, L. Gorb, J. Leszczynski, Determination of redox potentials for the Watson-crick base pairs, DNA nucleosides, and relevant nucleoside analogues, J. Phys. Chem. B 111 (2007) 5386–5395.

[45] A. Krittayavathananon, P. Iamprasertkun, M. Sawangphruk, Enhancing the charge-storage performance of N-doped reduced graphene oxide aerogel supercapacitors by adsorption of the cationic electrolytes with single-stand deoxyribonucleic acid, Carbon 109 (2016) 314–320.
[46] M. Pang, S. Jiang, J. Zhao, S. Zhang, R. Wang, N. Li, R. Liu, Q. Pan, W. Qu, B. Xing, Water-in-salt" electrolyte enhanced high voltage aqueous supercapacitor with carbon electrodes derived from biomass waste-ground grain hulls, RSC Adv. 10 (2020) 35545–35556.
[47] G.A. Ali, E. Megiel, J. Romański, H. Algarni, K.F. Chong, A wide potential window symmetric supercapacitor by TEMPO functionalized MWCNTs, J. Mol. Liq. 271 (2018) 31–39.
[48] Y. Shao, M.F. El-Kady, J. Sun, Y. Li, Q. Zhang, M. Zhu, H. Wang, B. Dunn, R.B. Kaner, Design and mechanisms of asymmetric supercapacitors, Chem. Rev. 118 (2018) 9233–9280.
[49] C.X. Guo, A.A. Chitre, X. Lu, DNA-assisted assembly of carbon nanotubes and MnO_2 nanospheres as electrodes for high-performance asymmetric supercapacitors, Phys. Chem. Chem. Phys. 16 (2014) 4672–4678.
[50] S.R. Ede, A. Ramadoss, S. Anantharaj, U. Nithiyanantham, S. Kundu, Enhanced catalytic and supercapacitor activities of DNA encapsulated β-MnO_2 nanomaterials, Phys. Chem. Chem. Phys. 16 (2014) 21846–21859.
[51] Z. Wu, A. Ono, M. Kainosho, A. Bax, H•••N hydrogen bond lengths in double stranded DNA from internucleotide dipolar couplings, J. Biomol. NMR 19 (2001) 361–365.
[52] B. Pal, S. Yang, S. Ramesh, V. Thangadurai, R. Jose, Electrolyte selection for supercapacitive devices: a critical review, Nanoscale Adv. 1 (2019) 3807–3835.
[53] G.A.M. Ali, E. Megiel, P. Cieciórski, M.R. Thalji, J. Romański, H. Algarni, K.F. Chong, Ferrocene functionalized multi-walled carbon nanotubes as supercapacitor electrodes, J. Mol. Liq. 318 (2020) 114064-114064.
[54] S.R. Shin, C.K. Lee, I.S. So, J.H. Jeon, T.M. Kang, C.W. Kee, S.I. Kim, G.M. Spinks, G.G. Wallace, S.J. Kim, DNA-wrapped single-walled carbon nanotube hybrid fibers for supercapacitors and artificial muscles, Adv. Mater. 20 (2008) 466–470.
[55] U. Nithiyanantham, A. Ramadoss, S. Kundu, Synthesis and characterization of DNA fenced, self-assembled SnO_2 nano-assemblies for supercapacitor applications, Dalton Trans. 45 (2016) 3506–3521.
[56] F. Zhang, H. Cao, D. Yue, Z. Zhou, Graphene covalently modified by DNA G-Base, J. Phys. Chem. C 117 (2013) 3513–3519.
[57] Y. Xue, T. Chen, S. Song, P. Kim, J. Bae, DNA-directed fabrication of $NiCo_2O_4$ nanoparticles on carbon nanotubes as electrodes for high-performance battery-like electrochemical capacitive energy storage device, Nano Energy 56 (2019) 751–758.
[58] G.A.M. Ali, O.A. Habeeb, H. Algarni, K.F. Chong, CaO impregnated highly porous honeycomb activated carbon from agriculture waste: symmetrical supercapacitor study, J. Mater. Sci. 54 (2019) 683–692.
[59] M.R. Thalji, G.A.M. Ali, P. Liu, Y.L. Zhong, K.F. Chong, $W_{18}O_{49}$ nanowires-graphene nanocomposite for asymmetric supercapacitors employing $AlCl_3$ aqueous electrolyte, Chem. Eng. J. 409 (2021) 128216, doi:10.1016/j.cej.2020.128216.
[60] P.T. Moseley, D.A.J. Rand, A. Davidson, B. Monahov, Understanding the functions of carbon in the negative active-mass of the lead–acid battery: a review of progress, J. Energy Storage 19 (2018) 272–290.